Research Article

Low-temperature synthesis of nanoscale $BaTiO_3$ powders via microwave-assisted solid-state reaction

Han-Sol Yun[1] · Byeong-Gyu Yun[1] · Hye-Min Lee[2] · Dae-Yong Jeong[1] · Wan-In Lee[2] · Nam-Hee Cho[1]

© Springer Nature Switzerland AG 2019

Abstract
Microwave-assisted solid-state reactions (MSSR) are investigated for their ability to synthesize nanocrystalline $BaTiO_3$ powders at low temperatures. $Ba(OH)_2{\cdot}H_2O$ and $TiO_2{\cdot}xH_2O$ are, respectively, initial precursors for Ba and Ti. In this study, these precursors were mixed according to their chemical stoichiometry and heated in a temperature range of 100–1000 °C by MSSR. Nanocrystalline $BaTiO_3$ powders having an average size of 26 nm were produced by MSSR, even at 100 °C. The crystallization-related activation energy for the formation of $BaTiO_3$ with the precursors by MSSR was ~ 9.6 kJ/mol, which is less than 1/10 of the value (120 kJ/mol) when the conventional solid-state reaction was applied. The nanostructural and physical features of the MSSR-based powders are compared with those prepared using the conventional solid-state reaction.

Keywords Barium titanate ($BaTiO_3$) · Microwave-assisted solid-state reaction · Activation energy · Nanostructural features

1 Introduction

Barium titanate ($BaTiO_3$) is one of the most attractive ferroelectric materials having a ABO_3-type perovskite structure. It is extensively used in electronic applications, including as multilayer ceramic capacitors, piezoelectric devices, thermistors with positive temperature coefficients, and semiconducting memory devices [1–3]. Various aspects of this material have been widely examined, including its synthesis, sintering, and nanostructural characteristics, to improve the dielectric properties of materials [3–5]. In particular, with the advent of nanotechnology, many researchers have investigated advanced synthesis methods to fabricate nano-sized $BaTiO_3$ powders having fine features and high crystallinity. These methods include solid-state reactions, sol–gel processes, and hydrothermal methods [6–8].

Solid-state reactions comprise the most common powder manufacturing process, owing to the simplicity of the preparation process and the low cost of source materials. However, the process often requires high temperatures and long reaction times to achieve a complete reaction, and the powders exhibit a large size of more than 500 nm [6, 9]. In contrast, the sol–gel process is usually carried out at low temperatures, which can be used to synthesize nano-sized powders. However, it requires a rather complicated process to produce the sol-type precursors, and the cost of some of its source materials are high. Additionally, the hydrothermal method can be used to synthesize nano-sized powders having good crystallinity. However, this method has some drawbacks, including slow kinetics and a limited reaction temperature below 300 °C because of the limits of the apparatus (e.g., Teflon vessels) [10–12].

It has been shown that the application of microwaves has the potential to enhance crystallization and densification kinetics in materials-engineering processes [13–15]. Microwave-assisted processes have various advantages, such as high power density, controllable penetration depth, rapid heating, and uniform heating of processed

✉ Nam-Hee Cho, nhcho@inha.ac.kr | [1]Department of Materials Science and Engineering, Inha University, Nam-gu, Incheon 22212, South Korea. [2]Department of Chemistry, Inha University, Nam-gu, Incheon 22212, South Korea.

SN Applied Sciences (2019) 1:1366 | https://doi.org/10.1007/s42452-019-1398-z

Received: 15 May 2019 / Accepted: 1 October 2019 / Published online: 10 October 2019

materials [16, 17]. In particular, no thermal conductivity mechanism has been associated with microwave heating, because microwave energy is transferred directly via electromagnetic fields into the materials [18]. Owing to these advantages, hybrid-type sol–gel processes and hydrothermal methods, including microwave irradiation, have been studied to control the crystallization of ceramic powders under various conditions.

Guo et al. [19] reported that 150-nm-sized $BaTiO_3$ powders had been synthesized at a reaction temperature of 80 °C using the microwave-assisted hydrothermal method, which is considered preferable to the conventional hydrothermal method, owing to its time savings, low temperature, and easy application. Sun et al. [20] confirmed that the application of microwaves via the hydrothermal method can control the structural features of synthesized $BaTiO_3$ powders with a short synthesis time. Malghe et al. [21] performed studies on the effects of microwaves when cubic-$BaTiO_3$ powders were synthesized at 500 °C via the sol–gel method, reporting that it contributed to transformation to the tetragonal phase in a microwave field above 700 °C.

There have only been a few studies on the application of microwaves in the formation of ceramic powders via solid-state reactions. Precursors having polar-type bonds provide potential for future application in microwave-assisted solid-state reactions [22, 23]. There has been little investigation on the detailed kinetics relevant to the microwave contribution.

In this study, we investigated how microwave-assisted solid-state reaction (MSSR) can be applied to fabricate nanoscale $BaTiO_3$ powders. The influence of the microwaves on the crystallization and growth of $BaTiO_3$ powders was studied in terms of initial precursors bearing hydroxides and water. The conventional heating-related activation energy was estimated to examine kinetics for the formation of the crystalline $BaTiO_3$ phase when the powders were prepared by MSSR. These results were compared with the values for $BaTiO_3$ powders prepared by conventional solid-state reactions (CSSR).

2 Experimental details

In this study, two types of Ba and Ti precursors were used. Initial precursors for Ba-source included $Ba(OH)_2{\cdot}H_2O$ (BH, JUNSEI, Japan) and $BaCO_3$ (BC, JUNSEI, Japan). The initial sources for Ti were $TiO_2{\cdot}H_2O$ (TH) and rutile-TiO_2 (TO, JUNSEI, Japan). Source TH was an amorphous titania synthesized by adding NH_4OH solution in a hydrolyzed $TiOCl_2$ solution. The solution was produced by reacting it with titanium tetrachloride ($TiCl_4$) and ice-cold deionized water at 60 °C for 1 h. The initial sources were made by mixing respective Ba and Ti precursors with a Ba/Ti mole ratio of 1:1. These mixed powders are BHTH (BH + TH), BHTO (BH + TO), BCTH (BC + TH), and BCTO (BC + TO). The four types of mixed powders were heat-treated at temperatures ranging from 100 to 1000 °C for 0–60 min via MSSR and CSSR. On the other hand, $BaTiO_3$ powders were also prepared by hydrothermal synthesis to compare structural features with those of the powders prepared by MSSR method. Barium hydroxide octahydrate ($Ba(OH)_2{\cdot}8H_2O$) and TH were used as source materials for Ba and Ti, respectively. Details of the hydrothermal process are listed in Ref. [24].

MSSR and CSSR processes were carried out at heating rates of 100 °C/min and 5 °C/min, respectively, and the samples were cooled naturally. The processing temperature was measured using a thermocouple placed near the sample within the hot zone in the furnace. The microwave heating furnace (Unicera Co., UMF-04), having a monomode reactor, was operated at a microwave frequency of 2.45 GHz and a power of 2 kW. The temperature was controlled using a micro-time slicing method of the microwave power. Conventional heating, however, was carried out with a power of 4 kW in an electrical furnace.

The crystallization and nanostructural features of $BaTiO_3$ powders were examined using X-ray diffraction (XRD; Rigaku, Multiflex 3 kW) using a Cu Kα line (λ = 1.5406 Å). A scan step size and scan speed were set to be 0.02° and 2°/min, respectively. The variation in nanocrystallite size (D) of the powders was measured by examining the XRD results using Scherrer's equation [25]:

$$D = 0.9\lambda/B\cos\theta, \quad (1)$$

where λ is the wavelength of the X-ray, B is the full width at half maximum (FWHM), and θ is the angle of the diffracted peak. To estimate the conventional heating-related activation energy for the formation of crystalline $BaTiO_3$, isothermal heat-treatments were carried out for 0^+, 10, and 60 min at 100–400 °C for MSSR and 600–900 °C for CSSR. Here 0^+ stands for the heat-treatment in which the sample was cooled immediately after the holding temperature was reached. The kinetics of the isothermal reaction for the formation of $BaTiO_3$ phase was estimated based on the Arrhenius method. Fourier transform Raman (FT-Raman; Bruker, RFS-100/S) was used to estimate the relative tetragonal fraction of the $BaTiO_3$ powders. The 1064-nm line of a Nd-YAG laser was used, and the applied power was set to be 20 mW. The morphological features were investigated using high-resolution scanning electron microscopy (HR-SEM; Hitachi, SU-8010). All images were obtained in the secondary electron mode, and the accelerating voltage was 15 kV.

3 Results and discussion

3.1 Synthesis of $BaTiO_3$ powders

In Fig. 1, the XRD patterns of the powders prepared using BHTH by the MSSR (Fig. 1a) and CSSR (Fig. 1b) methods for 60 min are illustrated. The presence and variation in nanocrystallite size of the $BaTiO_3$ phase were measured from the powders in terms of preparation temperature. Figure 1a shows that the $BaTiO_3$ phase was formed even at 100 °C by MSSR, and the intensity of the peaks related to the $BaTiO_3$ structure increased steadily to ~ 600 °C with increasing reaction temperatures. A small fraction of $BaCO_3$ was noticed under the preparation conditions. It was also noticed that the $BaTiO_3$ and Ba_2TiO_4 phases co-existed when the temperature reached 600 °C.

In contrast, for powders prepared via CSSR, as shown in Fig. 1b, $BaTiO_3$ phases started to form at ~ 600 °C. $BaCO_3$ phases were dominantly present at this temperature. The $BaTiO_3$ phase was produced at temperatures higher than 600 °C. As a result, in the temperature range of 700–1000 °C, $BaTiO_3$ phase existed dominantly. Figure 1c, d show the variation in the nanocrystallite size of the $BaTiO_3$ powders prepared using BHTH by MSSR and CSSR methods. The FWHM of diffracted peaks (101) is also illustrated in the figure. The nanocrystallite size of the powders synthesized at 100 °C by MSSR was 16 nm, and the size gradually increased to 27 nm with increasing synthesis temperature up to 600 °C. The value of FWHM gradually varied between 0.415 and 0.307 with temperature. On the other hand, in case of the powders prepared by the CSSR method, the nanocrystallite size increased from 42 to 58 nm at the reaction temperature ranging from 700 to 1000 °C. The value of FWHM gradually varied from 0.205 to 0.141 with temperature. To see the difference in how the precursors (e.g., BHTH) with hydroxide and/or water behave compared with those without polar-type bonds, BHTH, BHTO, BCTH, and BCTO were reacted at 400 °C for 60 min via MSSR.

Figure 2 shows the XRD results of the powders having the four different precursors. The $BaTiO_3$ phase was only

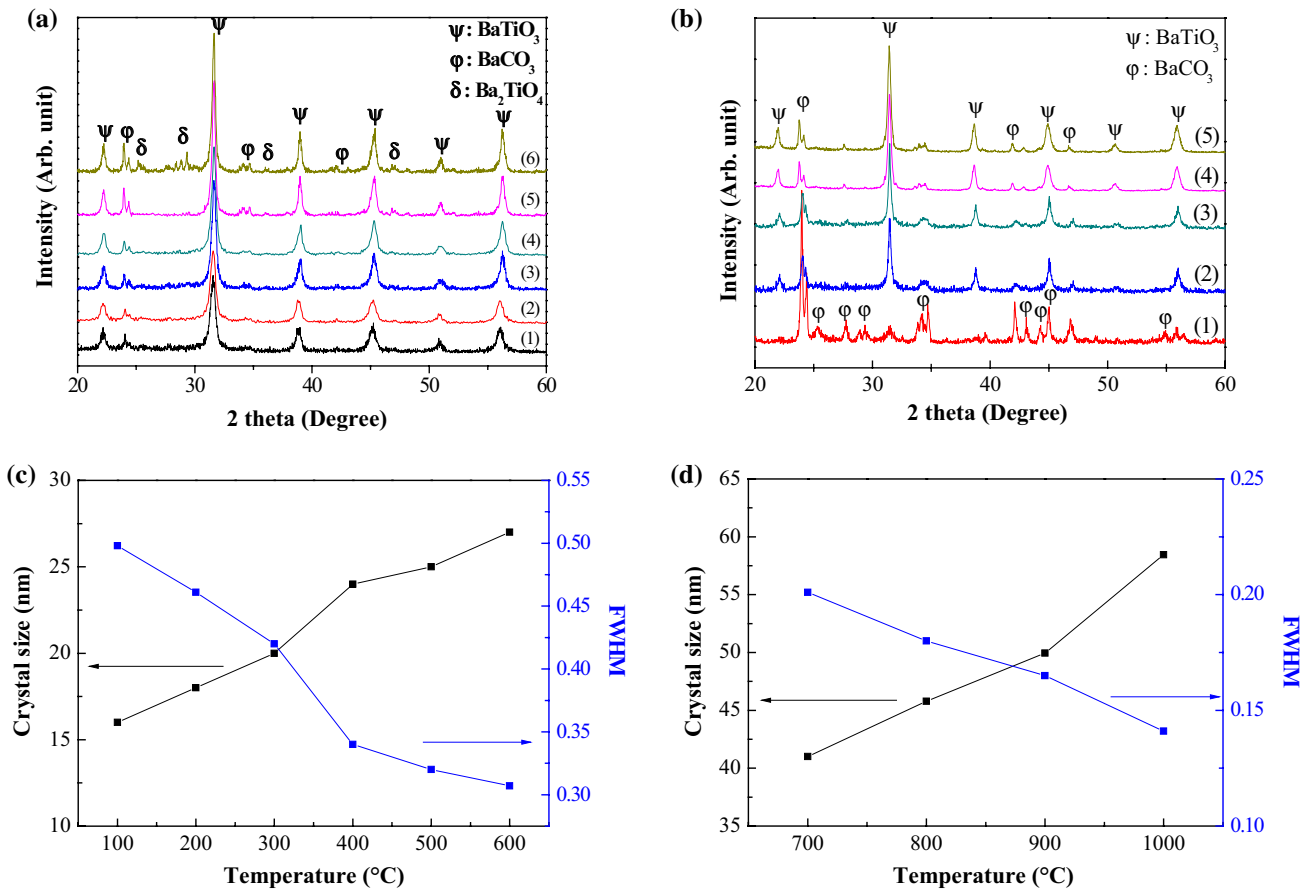

Fig. 1 XRD patterns of powders prepared with BHTH, synthesized at (1) 100 °C, (2) 200 °C, (3) 300 °C, (4) 400 °C, (5) 500 °C, and (6) 600 °C for 60 min by **a** MSSR and (1) 600 °C, (2) 700 °C, (3) 800 °C, (4) 900 °C, and (5) 1000 °C for 60 min by **b** CSSR. Variation in the FWHM of the (101) peaks and nanocrystallite sizes of the $BaTiO_3$ powders prepared with BHTH by **c** MSSR and **d** CSSR

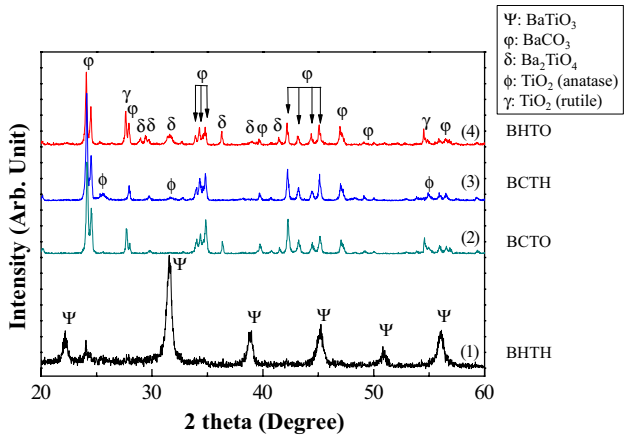

Fig. 2 XRD patterns of the powders prepared with (1) BHTH, (2) BCTO, (3) BCTH, and (4) BHTO. The samples were reacted at 400 °C for 60 min using the MSSR method

produced in powders prepared with BHTH, and a small fraction of the $BaCO_3$ phase was observed in the products. The nanocrystallite size of the $BaTiO_3$ structure was approximately 20 nm. In contrast, the powders prepared with BHTO exhibited $BaCO_3$ and rutile-TiO_2 phases with a little Ba_2TiO_4 phase. The powders synthesized using BCTH and BCTO showed only $BaCO_3$ and TiO_2 structures, indicating that no reaction took place between the Ba and Ti sources. The TiO_2 included anatase and rutile phases.

When BH reacted with TH or TO, new compounds such as $BaTiO_3$ and Ba_2TiO_4 phases were produced by the reaction between Ba and Ti ions, while a $BaCO_3$ phase was also produced as a by-product. The presence of $BaCO_3$ is likely to be attributed to the reaction of Ba ions with CO_2 in air. On the other hand, when the Ba source material was of $BaCO_3$ (BC), Ba and Ti ions reacted to a little degree at this temperature regardless of the type of Ti precursors. Instead, the phase transition related to the TiO_2 structure occurred so that some of the source rutile-type phases became an anatase phase [26].

In our experiments, for BH, Ba ions were bonded with hydroxide and/or the water was placed on the surface of Ba ions. For TH, Ti–O was chemically bonded with dihydrate placed on the surface of Ti ions. Zhao et al. [27] reported that the initial sources having water and/or hydroxide had high surface energies, resulting in high reactivity. As shown in Fig. 3, the initial sources with water and/or hydroxide molecules had higher free energy at 100 °C (state I) than that at room temperature (state II). The initial sources without any water and/or hydroxide (e.g., $BaCO_3$ and TiO_2) were expected to have the lowest free energy at room temperature (state III) among the source materials. Comparisons were made with respect to the transition states for the formation of $BaTiO_3$ in the figure. Therefore, the initial sources having water and/or hydroxide were expected to require a smaller energy for the formation of $BaTiO_3$.

Initial sources having additional polar dipoles (e.g., water (H_2O) and hydroxide (OH-)) were expected to have molecular oscillations under microwave irradiation [22, 28, 29]. Consequently, microwave-related energy is absorbed effectively in the materials, and it can decrease the conventional heating-related thermal energy barrier for the formation of a $BaTiO_3$ structure. In Fig. 3, the activated state was set for the formation of $BaTiO_3$, and, as a result, the initial source materials having water and/or hydroxide could overcome the energy barrier ($\Delta E_{a,1}$), even at 100 °C with the assistance of microwave (in Fig. 1a) energy. Here, the conventional heating-related energy at

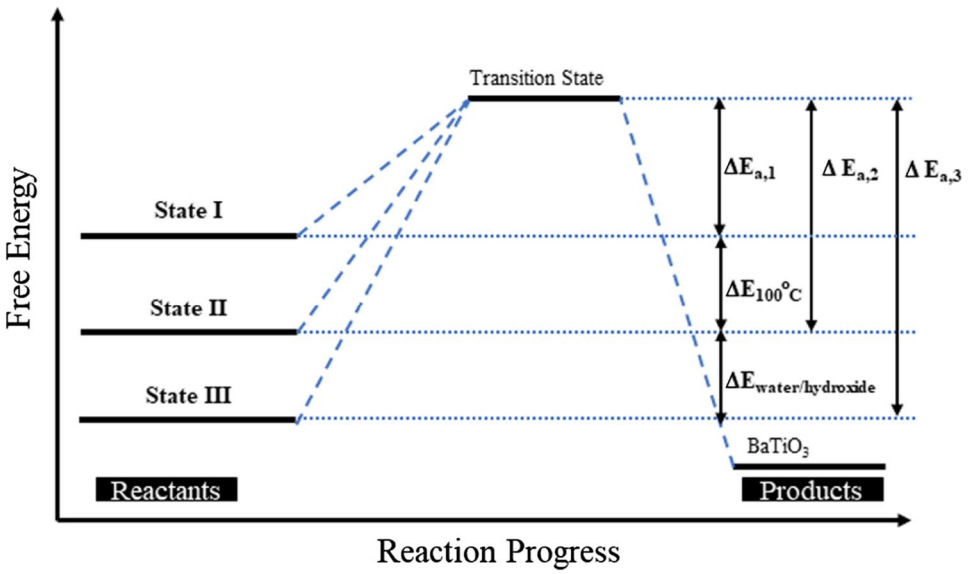

Fig. 3 Free energy states of initial sources with or without water and hydroxides. Schematic of the effective energy barrier for the formation of $BaTiO_3$. The barrier can be overcome via the application of microwave and thermal energy. States I and II represent free energies of reactants with water/hydroxide with the additional thermal energies of 100 °C and room temperature, respectively. State III indicates free energy of reactants without water/hydroxide at room temperature

this temperature is represented by $\Delta E_{100\,^{\circ}C}$, and the energy, which was conceived from the electromagnetic field, is regarded to be approximately $\Delta E_{a,1}$. These approximated values were made based on the lowest temperature at which the formation of $BaTiO_3$ was observed in Fig. 1a. On the contrary, in case of initial sources without water and hydroxide, the energy barrier of $\Delta E_{a,3}$ was higher than that of $\Delta E_{a,1}$, Therefore, the contribution from the microwave was negligible for overcoming $\Delta E_{a,3}$.

Similarly, TO had a lower reactivity than did TH by $\Delta E_{water/hydroxide}$. Owing to the low reactivity and the lack of additional polar dipoles of TO, BHTO had insufficient energy to overcome the activation energy for the formation of $BaTiO_3$, even at a reaction temperature of 400 °C (in Fig. 2).

3.2 Estimation of the crystallization activation energy for the formation of $BaTiO_3$ phase

The microwave effect on the crystallization of the $BaTiO_3$ structure was quantitatively investigated by calculating the conventional heating-related activation energy for the formation of the $BaTiO_3$ phase. The crystallization kinetics can be estimated in terms of nanocrystallite size by the following equation [30]:

$$G^n - G_0^n = k(t - t_0), \quad (2)$$

where G is the crystallite size of the $BaTiO_3$ structure, depending on the reaction time (t). G_0 is the initial size of crystallite for a reaction time of 0 + min (t_0), n is the crystallite growth exponent related to crystallization mechanism, and k is the reaction rate constant. The exponent (n) can be measured using a best-fit method from the logarithm of Eq. (2), as shown in the inset of Fig. 4a, b [31]. The values of n were determined to be 3.8 and 2.4 for the formation of $BaTiO_3$ phase using MSSR and CSSR methods, respectively. It was reported that the n value was significantly associated with the crystallization mechanism [32, 33]. The significant difference in the n values indicates that the growth of $BaTiO_3$ crystal in the MSSR method was dominantly dependent on the diffusion process of the constituents, whereas an interface movement was the determining process when CSSR was applied. More experimental investigation is under way to support the respective crystal-growth processes.

The conventional heating-related activation energy can be calculated by the Arrhenius equation, as follows:

$$\ln k = \ln k_0 - Q/RT, \quad (3)$$

where k is the reaction rate, k_0 is the pre-exponential constant, Q is the activation energy, R is the gas constant, and T is the absolute reaction temperature.

Based on the nanocrystallite size of the $BaTiO_3$ structure, the conventional heating-related activation energy (Q) for the phase formation can be calculated from the slope of the straight line fitted to a plot of ln k versus 1/T, as shown in Fig. 4c, d [34]. Table 1 shows that the value of ln k and the activation energies of BHTH heat-treated by MSSR at temperatures ranging from 100 to 400 °C and by CSSR at temperatures ranging from 700 to 1100 °C were calculated in terms of the reaction times 0^+–10 and 10–60 min, respectively. The respective ranges of the temperatures were confirmed to be the temperatures at which the $BaTiO_3$ phase was actively produced from BHTH by MSSR and CSSR (in Fig. 1).

The activation energy for a reaction time of 0^+–10 min was ~ 9.6 kJ/mol for BHTH prepared by MSSR, which is far less than that of BHTH prepared by CSSR (120 kJ/mol). The activation energies for BHTH samples prepared by MSSR and CSSR for 10–60 min slightly decreased to 8.3 and 115 kJ/mol, respectively.

There have been few reports about the estimation of the crystallization energy of $BaTiO_3$ based on Ba- and Ti- source materials having hydroxide or water. Therefore, it is not possible to make a direct comparison of our results with other research group's work. According to Osman [35], the activation energy for the formation of the $BaTiO_3$ phase based on the reaction between $BaCO_3$ and TiO_2 at temperatures of 970–1075 °C ranged from 183 to 197 kJ/mol. Additionally, Balaz et al. [36] reported that the activation energy for the formation of the $BaTiO_3$ phase by the reaction between $BaCO_3$ and TiO_2 at a temperature of 620 °C was approximately 270 kJ/mol. The values (183 and 270 kJ/mol) for the formation of the crystalline $BaTiO_3$ phase were much higher than 120 kJ/mol obtained in this study by CSSR for 0–10 min.

As in the case of BHTH, the energy barrier ($\Delta E_{a,2}$) was smaller than those ($\Delta E_{a,3}$) of initial sources without water and hydroxide. Thus, the activation energy for the formation of $BaTiO_3$ from BHTH by CSSR in this study was lower than that for the reaction between $BaCO_3$ and TiO_2 at a temperature of 620 °C [36]. Additionally, under microwave irradiation, BHTH prepared by MSSR had a significantly lower conventional heating-related activation energy value (9.6 kJ/mol) compared with BHTH prepared by CSSR. This difference indicated that the additional water molecules of the initial sources seemed to bring an excitation energy of ~ 110 kJ/mol to BHTH under microwave irradiation. Consequently, owing to the contribution of the microwave effect on the reaction, BHTH underwent an efficient synthesis process by MSSR resulting in the rapid synthesis of the $BaTiO_3$ phase, even at a low temperature of 100 °C and a short reaction time of less than 1 min.

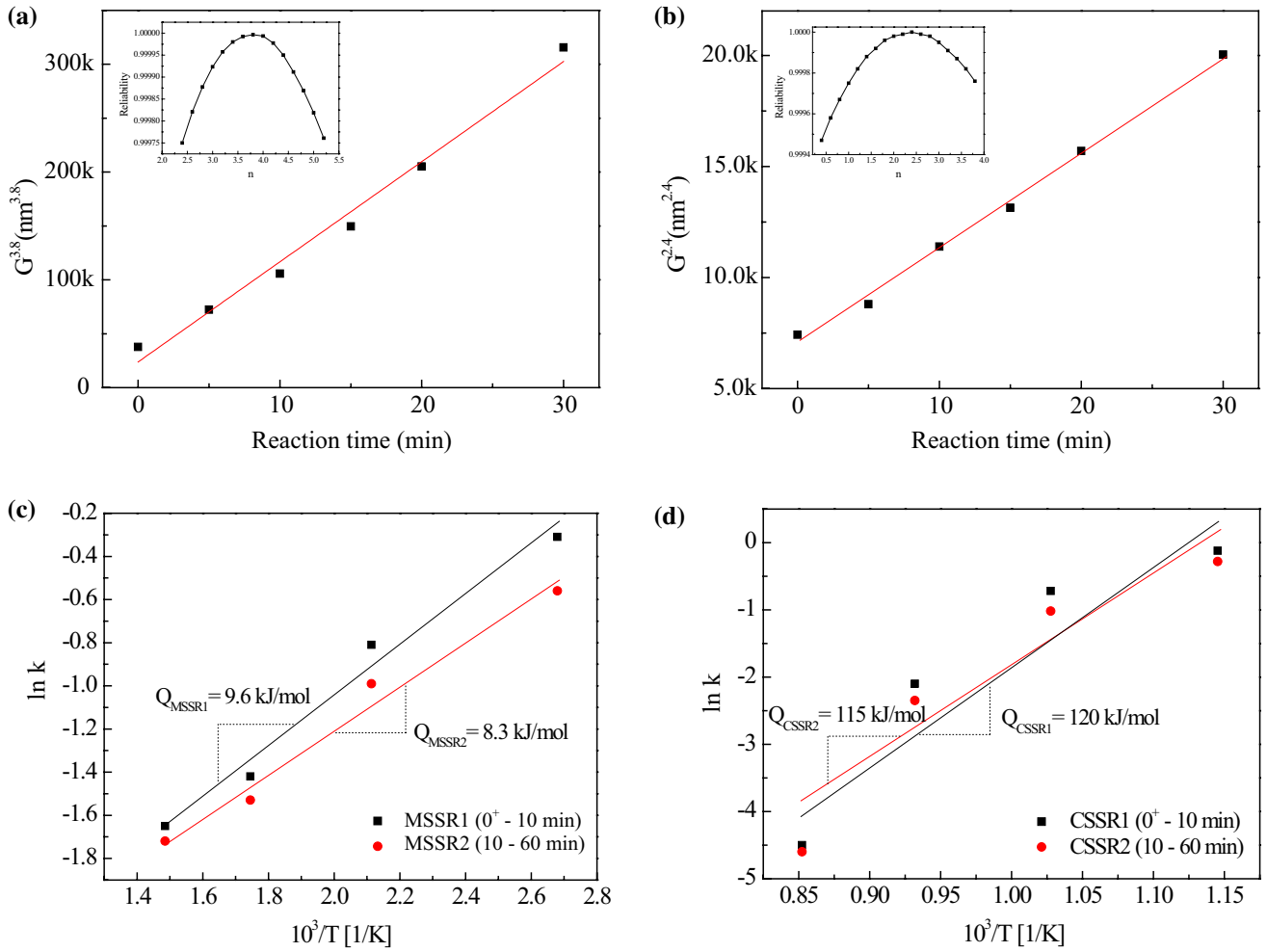

Fig. 4 Variations in crystallite size (D^n) of $BaTiO_3$ powders prepared by **a** MSSR and **b** CSSR methods are plotted in terms of holding time (t). The powders were synthesized at 100 °C by MSSR and at 700 °C by CSSR, respectively. Crystal growth exponent (n) was evaluated based on the best-fit method, as shown in the insets. Plots of ln k versus 10^3/T were used to calculate the crystallization activation energy of sample BHTH prepared by **c** MSSR and **d** CSSR methods

3.3 Microstructural and physical features of the $BaTiO_3$ powders prepared by various synthesis methods

Figure 5 shows the XRD results obtained from the powders prepared at 100 °C for less than 1 min with BHTH by MSSR and at 180 °C for 6 h by the hydrothermal method. These powders had the same crystal phases of $BaTiO_3$ and $BaCO_3$. These results indicate that the powders prepared by MSSR and hydrothermal methods had a similar crystallinity as that of the $BaTiO_3$ structure, and the powders prepared by MSSR had a lower fraction of the $BaCO_3$ phase than did the powders prepared by the hydrothermal method.

In Fig. 6, SEM images of the $BaTiO_3$ powders prepared with BHTH at 100 °C by MSSR, at 180 °C by the hydrothermal method, and at 600 °C by CSSR were measured to examine the size and shape of the powders. The powders prepared at 100 °C by MSSR have a spherical shape, appearing similar to that of the powders synthesized by the hydrothermal method. The size of the powders prepared by MSSR is ~ 26 nm, whereas that of powders prepared by hydrothermal method is ~ 54 nm. However, in Fig. 6c, the powders prepared by CSSR had an average size of ~ 320 nm, and the surface seemed to be faceted because of the crystal growth at a considerably high temperature (600 °C).

Figure 7 shows the FT-Raman spectra measured from the $BaTiO_3$ powders prepared at 100 °C by MSSR, at 600 °C by CSSR, and at 180 °C by the hydrothermal method. The intensity of the peak obtained from the powders near at 305 cm^{-1} was compared with the standard tetragonal-phased $BaTiO_3$ powders to estimate the relative tetragonal fraction of the powders [37]. The intensity of the peak was estimated by measuring the area under the peak after

Table 1 Crystallization activation energy of the MSSR and CSSR synthesis processes

Method	Soaking time (min)	Synthesis temperature (°C)	ln k	Q (kJ/mol)
MSSR1	0^{+}–10	100	−0.31	9.6
		200	−0.81	
		300	−1.42	
		400	−1.65	
MSSR2	10–60	100	−0.56	8.3
		200	−0.99	
		300	−1.53	
		400	−1.72	
CSSR1	0^{+}–10	600	−0.12	120
		700	−0.72	
		800	−2.1	
		900	−4.50	
CSSR2	10–60	600	−0.28	115
		700	−1.02	
		800	−2.35	
		900	−4.60	

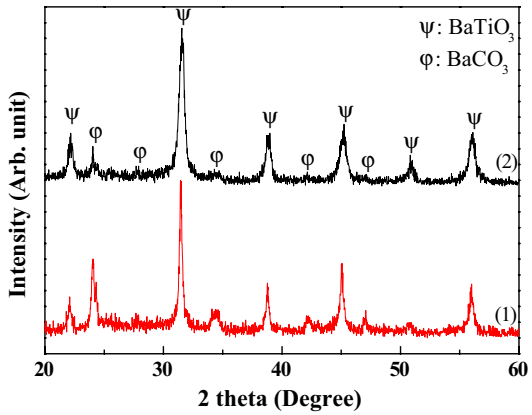

Fig. 5 XRD patterns of the powders prepared by the (1) hydrothermal and (2) MSSR methods

setting the baseline. The intensity ratios of the powders prepared by MSSR, CSSR, and the hydrothermal method were approximately 19%, 17%, and 12%, respectively.

4 Conclusions

$BaTiO_3$ powders having an average size of ~ 26 nm were formed at even 100 °C via MSSR. $Ba(OH)_2{\cdot}H_2O$ and $TiO_2{\cdot}xH_2O$ were used as Ba and Ti source materials, respectively. The crystallization kinetics of the $BaTiO_3$ phase were examined by estimating the conventional heating-related activation energies. The values for the synthesis of $BaTiO_3$ powders from $Ba(OH)_2{\cdot}H_2O$ and $TiO_2{\cdot}xH_2O$ by MSSR and CSSR were 9.6 and 120 kJ/mol, respectively. This result clearly shows that MSSR was an efficient synthesis process when initial source materials having water and/or hydroxide are used. Their additional polar molecules brought high reactivity under microwave irradiation.

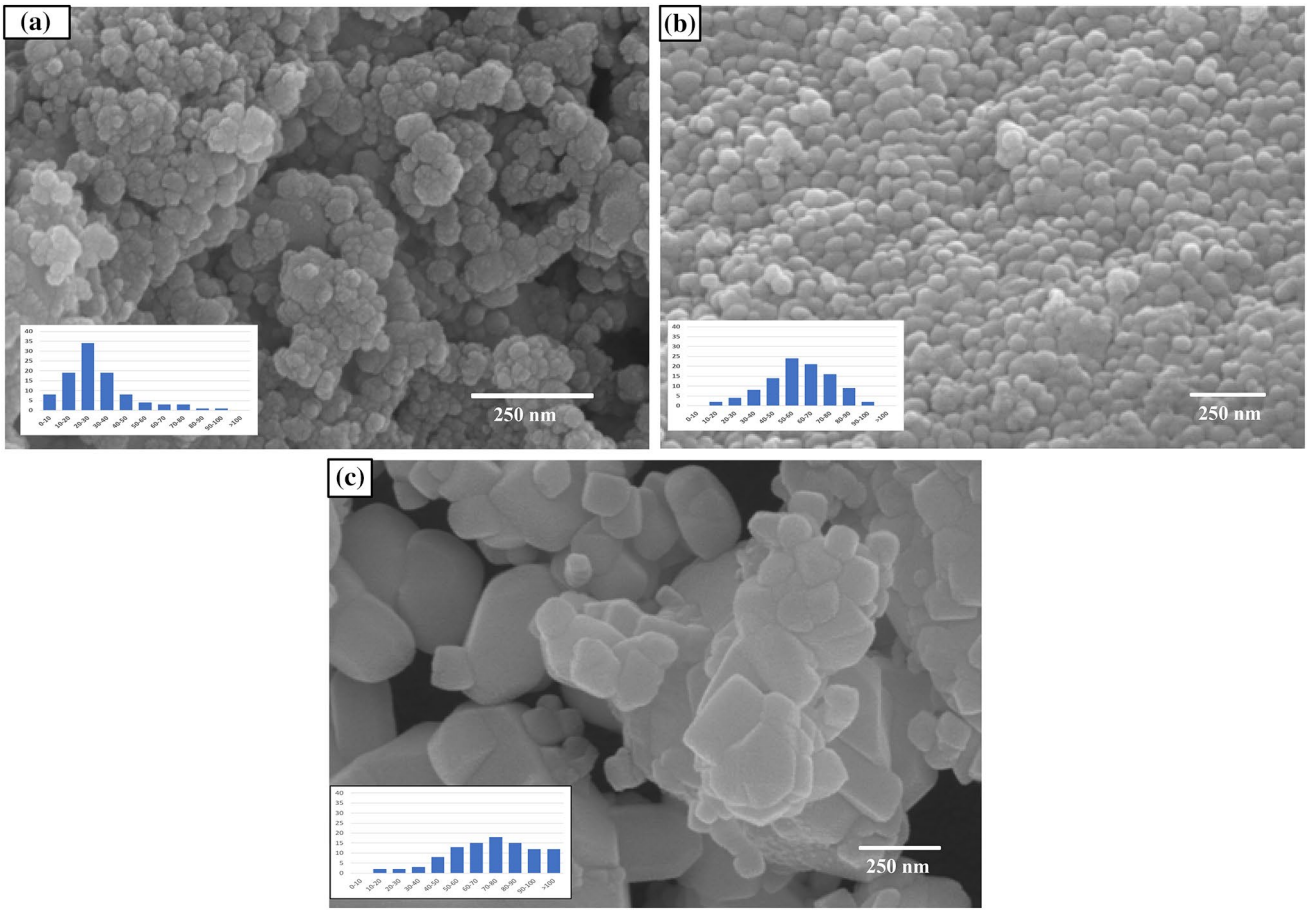

Fig. 6 SEM images were obtained from the powders prepared with BHTH, which were prepared by **a** MSSR at 100 °C, **b** the hydrothermal method at 180 °C, and **c** CSSR at 600 °C; size distribution of synthesized powders is shown in the insets

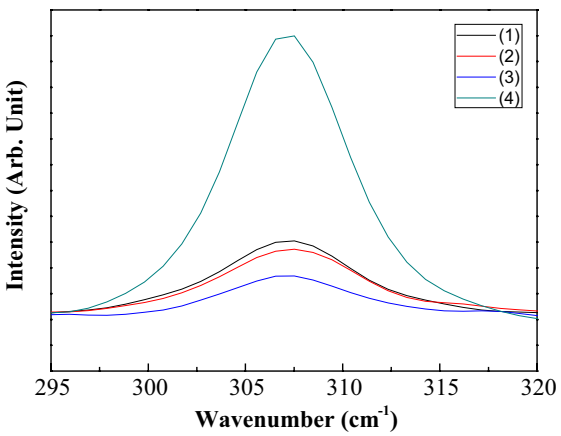

Fig. 7 FT-Raman spectra of $BaTiO_3$ powders prepared with BHTH, which was synthesized by (1) MSSR at 100 °C, (2) CSSR at 600 °C, (3) hydrothermal method at 180 °C, and (4) tetragonal-phased powders were commercially purchased

Funding This research was supported by the Basic Science Research Program through the National Research Foundation of Korea (NRF) funded by the Ministry of Education (2016R1D1A1B03934622).

Compliance with ethical standards

Conflict of interest The authors declare that they have no conflict of interest.

References

1. Kishi H, Mizuno Y, Chazono H (2003) Base-metal electrode-multilayer ceramic capacitors: past, present and future perspectives. Jpn J Appl Phys 42:1–15
2. Yang WC, Hu CT, Lin IN (2004) Effect of Y_2O_3/MgO Co-doping on the electrical properties of base-metal-electroded $BaTiO_3$ materials. J Eur Ceram Soc 24:1479–1483
3. Kwei GH, Lawson AC, Billinge SJL, Cheong SW (1993) Structures of the ferroelectric phases of barium titanate. J Phys Chem 97:2368–2377
4. Hu D, Ma H, Tanaka Y, Zhao L, Feng Q (2015) Ferroelectric mesocrystalline $BaTiO_3$/$SrTiO_3$ nanocomposites with

enhanced dielectric and piezoelectric responses. Chem Mater 27:4983–4994
5. Pena MA, Fierro JLG (2001) Chemical structures and performance of perovskite oxides. Chem Rev 101:1981–2017
6. Manzoor U, Kim DK (2007) Synthesis of nano-sized barium titanate powder by solid-state reaction between barium carbonate and titania. J Mater Sci Technol 23:655–658
7. Lemoine C, Gilbert B, Michaux B, Pirard JP, Lecloux A (1994) Synthesis of barium titanate by the sol–gel process. J Non-Cryst Solids 175:1–13
8. Lu SW, Lee BI, Wang ZL, Samuels WD (2000) Hydrothermal synthesis and structural characterization of $BaTiO_3$ nanocrystals. J Cryst Growth 219:269–276
9. Buscaglia MT, Bassoli M, Buscaglia V, Alessio R (2005) Solid-state synthesis of ultrafine $BaTiO_3$ powders from nanocrystalline $BaCO_3$ and TiO_2. J Am Ceram Soc 88:2374–2379
10. Boulos M, Guillemet-Fritsch S, Mathieu F, Durand B, Lebey T, Bley V (2005) Hydrothermal synthesis of nanosized $BaTiO_3$ powders and dielectric properties of corresponding ceramics. Solid State Ion 176:1301–1309
11. Shandilya M, Rai R, Singh J (2016) Review: hydrothermal technology for smart materials. Adv Appl Ceram 115:354–376
12. Komarneni S (2003) Nanophase materials by hydrothermal, microwave-hydrothermal and microwave-solvothermal methods. Curr Sci 85:1730–1734
13. Brosnan KH, Messing GL, Agrawal DK (2003) Microwave sintering of alumina at 2.45 GHz. J Am Ceram Soc 86:1307–1312
14. Srilakshmi C, Saraf R, Prashanth V, Rao GM, Shivakumara C (2016) Structure and catalytic activity of Cr-doped $BaTiO_3$ nanocatalysts synthesized by conventional oxalate and microwave assisted hydrothermal methods. Inorg Chem 55:4795–4805
15. Clark DE, Folz DC, West JK (2000) Processing materials with microwave energy. Mater Sci Eng 287:153–158
16. Stein DF (1994) Microwave processing of materials. National Academies Press, Washington
17. Booske JH, Cooper RF, Freeman SA (1997) Microwave enhanced reaction kinetics in ceramics. Mater Res Innov 1:77–84
18. Katz JD (1992) Microwave sintering of ceramics. Annu Rev Mater Sci 22:153–170
19. Guo L, Luo H, Gao J, Guo L, Yang J (2006) Microwave hydrothermal synthesis of barium titanate powders. Mater Lett 60:3011–3014
20. Sun W, Li C, Li J, Liu W (2006) Microwave-hydrothermal synthesis of teteragonal $BaTiO_3$ under various conditions. Mater Chem Phys 97:481–487
21. Malghe YS, Gurjar AV, Dharwadkar SR (2004) Synthesis of $BaTiO_3$ powder from barium titanyl oxalate (BTO) precursor employing microwave heating technique. Bull Mater Sci 27:217–220
22. Tsakalakos T, Ovid`ko IA, Vasudevan AK (2012) Nanostructures: synthesis, functional properties and applications. Kluwer Academic Publishers, Dordrecht
23. Gabriel C, Gabriel S, Grant EH, Halstead BSJ, Mingos DMP (1998) Dielectric parameters relevant to microwave dielectric heating. Chem Soc Rev 27:213–223
24. Moon SM, Lee CM, Cho NH (2006) Structural features of nanoscale $BaTiO_3$ powders prepared by hydro-thermal synthesis. J Electroceram 17:841–845
25. Patterson A (1939) The Scherrer formular for X-ray particle size determination. Phys Rev 56:978–982
26. Lee SI, Randall CA (2007) Modified phase diagram for the barium oxide-titanium dioxide system for the ferroelectric barium titanate. J Am Ceram Soc 90:2589–2594
27. Zhao G, Schwartz Z, Wieland M, Rupp F, Geis-Gerstorfer J, Cochran DL, Boyan BD (2005) High surface energy enhances cell response to titanium substrate microstructure. J Biomed Mater Res A 74:49–58
28. Bilecka I, Niederberger M (2010) Microwave chemistry for inorganic nanomaterials synthesis. Nanoscale 2:1358–1374
29. Kappe CO (2004) Controlled microwave heating in modern organic synthesis. Angew Chem Int Ed 43:6250–6284
30. Avrami M (1939) Kinetics of phase change I. J Chem Phys 7:1103–1112
31. Muthuramalingam M, Jain Ruth DE, Veera Gajendra Babu M, Ponpandian N, Mangalaraj D, Sundarakannan B (2016) Isothermal grain growth and effect of grain size on piezoelectric constant of Na 0.5 Bi 0.5 TiO 3 ceramics. Scr Mater 112:58–61
32. Coble RL (1961) Sintering crystalline solids. II. Experimental test of diffusion models in powder compacts. J Appl Phys 32:793–799
33. Iverson RB, Reif R (1987) Recrystallization of amorphized polycrystalline silicon films on SiO_2: temperature dependence of the crystallization parameters. J Appl Phys 62:1675–1681
34. Chen CS, Chen PY, Chou CC, Chen CS (2012) Microwave sintering and grain growth behavior of nano-grained $BaTiO_3$ materials. Ceram Int 38:S117–S120
35. Osman KI (2011) Synthesis and Characterization of $BaTiO_3$ Ferroelectric Material. PhD Thesis, Cairo University, Egypt
36. Balaz P, Plesingerova B (2000) Thermal properties of mechanochemically pretreated precursors of $BaTiO_3$ synthesis. J Therm Anal Calorim 59:1017–1021
37. Preda L, Courselle L, Despax B, Bandet J, Ianculescu A (2001) Structural characteristics of RF-sputtered $BaTiO_3$ thin films. Thin Solid Film 389:43–50

Publisher's Note Springer Nature remains neutral with regard to jurisdictional claims in published maps and institutional affiliations.